Anti-Tumor Potential of AEV01 in Glioma: In Vitro and Xenograft Model Studies.

Anitha TS[1], Indrani Biswas[2], Aravinda Kumar[3], MM Sekhar[4], Renu Medasani[4]

[1]Assistant Professor, Department of Biochemistry & Molecular Biology School of Life Sciences, Pondicherry University, Puducherry.

[2]Research Scholar, Mahatma Gandhi Medical Advanced Research Institute, Sri Balaji Vidyapeeth University, Puducherry

[3]Associate Professor, Department of Pharmacology, Pondicherry Institute of Medical Sciences, Ganapathichettikulam, Puducherry.

[4]Astrel Genome Ltd, Hyderabad, India

Abstract:

Background: Gliomas are difficult to treat with short survival rates despite current therapies. The need for new treatments is urgent, and orthotopic cell-derived tumor xenograft (CDX) models have provided valuable insights. AEV01, a specialty extract from the roots of Picrorhiza kurroa, shows promise as a non-surgical treatment option with anti-inflammatory, antioxidant, and anti-cancer properties. Its efficacy has been demonstrated in a patient with pancreatic cancer and in enhancing immune conditions in COVID-19 patients.

Objectives: This study was conducted with the objective to investigate the anti-tumour properties of AEV01 in human glioblastoma through in vitro and in vivo experiments.

Methodology: The methodology of the study involved the use cell lines namely HEK-293T and U-87 MG glioblastoma. The cytotoxicity of the drug AEV01 was assessed using the MTT assay. Dual staining with acridine orange/ethidium bromide was performed to evaluate morphological changes in the cancer cells. ELISA was used to detect protein marker expression levels. Immunocytochemistry was employed to assess CD36 expression in various cellular models. Orthotopic tumor engraftment was carried out to establish a glioblastoma-induced model. Animal grouping and treatment plans were done, and histopathological effects were evaluated. Immunohistochemistry was performed to assess the anti-tumor effects of AEV01. ELISA and toxicity studies were also conducted.

Results: The results of the study showed that AEV01 had dose-dependent cytotoxicity against glioma, while minimally impacting normal cells. AEV01 induced apoptosis in cancer cells and downregulated the expression of inflammatory markers while upregulating the expression of the tumor suppressor protein TP53. AEV01 also decreased the expression of CD36, a potential target for cancer therapy, in glioma cancer cells. In an in vivo glioma-induced model, AEV01 exhibited anti-tumor effects and reduced the expression of CD36. Histopathological analysis demonstrated that AEV01 had minimal toxicity on vital organs. Overall, these findings suggest that AEV01 has potential as a therapeutic agent for glioma.

Introduction

Gliomas pose significant challenges in medical treatment, with a very short median survival and high recurrence rates despite existing therapies (1,2). The limited success of standard-of-care drugs and the scarcity of medical interventions and trials underscore the urgent need for novel therapeutic approaches. Orthotopic cell-derived tumor xenograft (CDX) model have provided valuable insights into the complex biology of gliomas (3), aiding in the identification of new therapeutic targets.

In response to this pressing need, AEV01 (a drug product from Astrel Genome Ltd, Hyderabad, India) is a novel specialty extract from the roots/rhizome extract of *Picrorhiza kurroa*, offers a promising avenue for non-surgical treatments. *Picrorhiza kurroa* is an important alpine herb of the Himalayan region, growing in an altitudinal range of 3000–5000 m in temperate belts. In the realm of Indian medicine, *Picrorhiza kurroa*, known as "Kutki" in Indian medicine, has a rich history and is renowned for its anti-inflammatory, antioxidant, hepatoprotective, immunostimulant, neuroprotective, and anti-cancer properties (4,5). Recently, AEV01 has shown remarkable efficacy in a 68-year-old patient with metastatic pancreatic cancer, demonstrating pain relief, increased energy, and improved chemotherapy recovery within weeks. Notably, blood markers were normalized, weight gain occurred, and T-cell function was fully rejuvenated over a two-month period, leading to a normal, active life (unpublished data). Moreover, Balan et al., in a recent randomized, placebo-controlled, double-blinded investigation, evaluated the safety and efficacy of AEV01 against COVID-19. Notably, AEV01 enhanced the immune conditions of COVID-19 patients, reducing NLR and CD4+/CD8+ T cell populations, thereby restoring vaccination efficacy in aged adults (6). This not only highlights the potential of AEV01 in combating viral infections but also suggests its broader applicability in human cancer treatment.

Therefore, with its broad potential in cancer therapy, this study seeks to investigate the anti-tumor properties of AEV01 in U-87MG (Human Glioblastoma), both through *in vitro* experiments and in an *in vivo* xenograft-induced animal model.

Materials and Methods

Chemicals

3-(4,5-dimethylthiazolyl-2)-2,5-diphenylte-trazolium bromide (MTT), DAPI (4′,6-diamidino-2-phenylindole), and all the other reagents used for the experiments were obtained from Sigma (USA) and HiMedia (Mumbai, India).

Cell Line and culture conditions

HEK-293T (Human embryonic kidney cell line) (Passage No: 10), U-87 MG human glioblastoma (GB) cell line (Passage Number: 58), HepG2 human liver cancer cell line (RRID: CVCL_GP63) (Passage Number: 58), Hep3B (Passage Number: 35) and WRL-68 liver senescence cells (Passage Number: 68) were procured from National Centre for Cell Sciences (NCCS) (Pune, India). HEK-293T, HepG2, Hep3B and WRL-68 cells were grown in Dulbecco's Modified Eagle's Medium (DMEM) with 10% FBS and 1% penicillin/streptomycin, while, U-87 MG human GB cell lines were maintained in Minimal Essential Medium Eagle (EMEM) with 10% FBS and 1% penicillin/streptomycin. The cells were sustained at 37ºC under humidified 5% CO_2 - 95% O_2. At their logarithmic growth phase, the cells were trypsinized, counted using trypan blue dye-exclusion method and resuspended in 1X-PBS to a final concentration of 1×10^6 cells per 3 µl of PBS.

Cytotoxicity Analysis- MTT assay

At their logarithmic growth phase, the cells were harvested using 0.25% Trypsin and 0.53 mM EDTA, counted by trypan-blue dye exclusion assay and seeded in 96-well plates at a density of 5×10^3 cells/well. After 24 hours of seeding, the cells were washed with 1X-PBS and treated with varying concentrations of the drug and vehicle control (VC) (100, 200, 300 and 400 µg) respectively for 24 hours. Post-treatment, the media was aspirated and 20 µl of MTT (5 mg/ml) reagent was added to each well and the cells were incubated in dark at 37ºC for 4 hours. To dissolve the purple formazan crystals formed, DMSO was added to each well. The absorbance at 570 nm was recorded using ELISA-Multiplate reader (Molecular Devices Spectra-Max M5, USA) and the absorbance values were obtained. To perform relative quantification, absorbance obtained from each group was normalized to that of the control group. The percentage viability was calculated using the formula:

% Viability = [(Optical density {OD} of treated cell − OD of blank)/ (OD of control − OD of blank) × 100].

Dual Staining of AEV01

Acridine orange/ethidium bromide (AO/EtBr) dual staining was carried out to validate if any morphological changes induced by AEV01 in these cancer cells. The drug was administered on U-87MG and HepG2 cells for 24 hours at 37°C, after being seeded in a 24-well plate at a density of $20x10^3$ per well. After incubation, cells were rinsed with 1XPBS, stained at room temperature, with 200µl of AO/EtBr (100 µg/ml AO and 100 µg/ml of EtBr) for 5 minutes. The stained cells were visualized using Fluorescent microscope (Axiovert 40 CFL, Germany) with an excitation wavelength of 300–360 nm. Images were quantified using Image J software. The stained cells were quantified using the following formula: % apoptotic cells = (number of apoptotic cells/total number of cells) □100.

ELISA

To detect the expression levels of protein markers namely, TNF-α (Catalogue No. O13850), IL-1β (Catalogue No. O12108), IL-18 (Catalogue No. O12104), CRP (Catalogue No. O11896), CASP-1 (Catalogue No. O10771), IL-6 (Catalogue No. O12137) and tumor protein TP53 (Catalogue No. O12769) using respective ELISA kits, procured from Origin Diagnostics & Research, Kerala, India. ELISA was performed according to the manufacturer's protocol. Briefly, the protein lysates obtained from various experimental groups were loaded in the 96-well plates. After removal of the unbound samples by wash buffer, 100 µl HRP-conjugated secondary was added to all the wells and the solution was incubated for 60 minutes at 37ºC. Following, 50 µl of substrate A and substrate B was added to each well (incubation at 37ºC for 30 minutes). To stop the reaction, 50 µl of stop solution was added to each well and the absorbance was measured at 450 nm immediately using spectrophotometer (Molecular Devices Spectra-Max M5, USA). Relative protein concentrations were then determined by interpolating the absorbance with that of the standard curve obtained from the standard protein.

Immunocytochemistry (ICC) of CD36 Expression in Various Cellular Models:

U-87MG and HepG2 cells were initially seeded in a 30-mm culture plate at a concentration of 8×10^3 cells, followed by fixation with 4% paraformaldehyde after 24 hours of incubation. Subsequent steps included permeabilization with Triton X 100, blocking with 3% BSA, and incubation with the primary CD36 antibody (Catalogue No. E-AB-33662, Elabsciences, Wuhan, China) at a 1:300 dilutions in 3% blocking buffer. After two washes with 1X PBS, the cells were subjected to a secondary FITC-conjugated antibody (Catalogue No. E-AB-

1014, Elabsciences, Wuhan, China) and counter-stained with DAPI. The process was observed and documented using a Fluorescence microscope (Axiovert 40 CFL, Germany).

Additionally, immunocytochemistry was employed to assess CD36 expression in HepG2 liver cancer cells under palmitic acid (PA) treatment conditions. Cells were seeded in a 24-well plate, treated with PA at 12.5 µg/ml and 50 µg/ml doses, individually and in combination with AEV01 at its IC50. The experimental procedure mirrored that of U-87MG and HepG2 cells, with fluorescence microscopy capturing the stained cells.

Furthermore, CD36 expression in WRL-68 liver senescence cells was examined using the same ICC protocol. The cells were seeded, fixed, permeabilized, and blocked before undergoing CD36 antibody incubation, secondary antibody treatment, and DAPI counterstaining. The resulting stained cells were then visualized and imaged using the Fluorescence microscope (Axiovert 40 CFL, Germany).

Establishment of U-87 MG human glioblastoma (GB) induced model

Healthy male Wistar rats (180–240 g) were obtained from Biogen Laboratories, Bangalore, India. Animals were housed in cages under optimum light conditions (12:12 h light–dark cycle), temperature (22 ± 1°C), and humidity (50 to 60%), with food and water provided *ad libitum*. All procedures used in the present study followed the CPSEAC guidelines, approved by the Institutional Animal Ethics Committee (IAEC No. 02/IAEC/MGMPRC/01/2023-II dated 29.8.2023 Sri Balaji Vidyapeeth, Puducherry). All efforts were made to minimize the number of animals and their suffering.

Intracranial tumor engraftment

To orthotopically implant glioma cells into healthy rats, stereotactic surgery was carried out according to the protocol. For this, the xenograft recipient was sedated using ketamine and xylazine cocktail (87 mg/kg and 13 mg/kg body weight). The skull was exposed by incising the skin from the frontal to the occipital bone. After marking the implantation location (3.00 mm lateral and 0.5 mm posterior position), a small burr hole was drilled using a cordless power drill. Following, a total of 1×10^6 C6 cells suspended in 3 µl PBS were delivered into the target site at a depth of 6 mm. The burr hole was then sealed with bone wax and appropriate post-operative relief measures were carried out.

Animal grouping and Treatment plan

20 days' post tumor implantation and affirming by histopathological examination, animals were randomly sub-divided into different categories as shown below:

S.No.	Experimental groups	No. of animals for glioma	No. of animals for HCC	Route of administration	Dosage
1	Group I- Untreated control group	6	6	NA	NA
2	Group II- tumour-induced, untreated	6	6	NA	NA
3	Group III- tumor-induced, AEV01-treated	6	6	Oral	41.33 mg/kg/day
4	Group IV- Tumor-induced, vehicle-treated	6	6	Oral	41.33 mg/kg/day

Histopathological effects of AEV01 in glioma-induced and HCC-induced xenograft model

All experimental groups' brain and liver tissues were separated, embedded in paraffin, and sectioned (4 µm) after being fixed in 10% formalin. H&E was used to stain the tissue sections. Inverted microscope (Primo Star, Carl Zeiss, Germany) was used to take microscopic pictures of the stained sections at a 40x magnification. ImageJ software was then used to quantify the images.

Immunohistochemistry of CD36

Immunohistochemistry (IHC) analysis was performed to assess the anti-tumor effects of AEV01 at molecular levels, against each of the experimental groups. Tissue sections from each experimental group were formalin-fixed and sectioned (5 µm). Following deparaffinization, formalin-fixed sections were heated in microwave for 20 minutes in sodium citrate buffer containing 10 mM sodium citrate and 0.05% Tween-20 (pH 6.0) to retrieve the antigen. Endogenous peroxidase activity was blocked by incubating the tissues in 3% H_2O_2 for 15 minutes. The tissue sections were then blocked with 3% bovine serum albumin (BSA) for 10 minutes. After washing in 1X-TBST buffer twice, the slides were sequentially incubated with primary antibodies (rabbit anti-CD36 antibody 1:100 dilution) for 1 hour at room temperature; After washing off the unbound antibodies, HRP-conjugated secondary antibody incubation for each of the sections was executed for 30 minutes at room temperature. The bound antibodies were detected using diaminobenzidine (DAB), counterstained with haematoxylin and mounted using mounting medium (Dako, Denmark).

Microscopic images were obtained using inverted microscope (Primo Star, Carl Zeiss, Germany). Positive expression of CD36 against each of the experimental groups has been interpreted in terms of immunoreactive scores (IRS) as listed in Table 1.

ELISA

ELISA was performed as mentioned above in the *in vitro* studies.

Toxicity studies against Glioma and HCC model

To evaluate if AEV01 induced toxicity against the vital organs, animals were sacrificed from AEV01-treated, glioma and liver-induced rats and each of these organs-heart, lungs, liver, kidney, spleen and pancreas were removed by a mid-line incision in the abdomen. These organs were formalin fixed, embedded in paraffin, sectioned and subjected to histopathological evaluation. Images were captured at 40X magnification and quantified using ImageJ.

Statistical Analysis

All the experiments were conducted in triplicates. Analysis of the experimental data was carried out using GraphPad Prism v.8.0.1 (GraphPad Software, San Diego, CA, USA). Results were represented as mean ± standard deviation (SD). Statistical analysis between the control and various experimental groups was performed using Analysis of Variance (ANOVA). $p < 0.05$ was considered to be significant.

Results

Dose-Dependent Cytotoxicity of AEV01 in Glioma and Liver Cancer Cells, with Minimal Impact on Normal Cells

The cytotoxicity of AEV01 was examined in both U-87 MG glioblastoma (GB) and HepG2 liver cancer cells through MTT assay. Across all selected concentrations, the drug demonstrated a significant and dose-dependent inhibition of cell growth. Notably, the most potent effective concentrations against the GB and liver cancer cell lines were observed at 300 µg and 400 µg of AEV01, respectively (Figure 1, I and II).

Additionally, the assessment extended to normal human embryonic kidney transformed cells, specifically the HEK-293T cell line, to ascertain the toxicity or tolerance of AEV01. The MTT assay results (Figure 1, III) indicated that AEV01 did not exhibit significant

cytotoxicity in these normal cells. This dual evaluation suggests the potential specificity of AEV01 in targeting cancer cells while maintaining a tolerable profile in normal cells.

AEV01-Induced Apoptosis in Glioma and Liver Cancer Cells

Building upon the cytotoxicity findings, the induction of apoptosis by AEV01 at concentrations of 300 µg and 400 µg was examined at the morphological level in U-87MG glioblastoma and HepG2 liver cancer cells using AO/EtBr dual stain. AO, permeable to live cells, appears green or yellow-green in early apoptosis, while EtBr stains dead cells in the late stage of apoptosis with orange-red fluorescence.

In this study, treatment with AEV01 significantly induced apoptosis in both U-87MG and HepG2 cells, with respective percentages of 24.5% and 59.59%. Intriguingly, the vehicle-control (VC, Figure 2: I and IIC) revealed that more than 90% of cells were live in both U-87MG and HepG2 cells, indicating that the vehicle-control did not induce apoptosis, at least to a significant extent. This morphological assessment aligns with the cytotoxicity data, reinforcing AEV01's potential as an inducer of apoptosis in cancer cells while sparing normal cells.

AEV01 Treatment Effects on Inflammatory and Tumor Protein Markers in Glioma and Liver Cancer Cells

In alignment with the observed significant induction of apoptosis in the dual-staining results, the current study investigated the impact of AEV01 at the protein expression level using ELISA. The results revealed that AEV01-treated glioma and liver cancer cells exhibited a downregulation in the expression of inflammatory markers, including IL-6, IL-18, IL-1β, TNF-α, CRP, and CASP-1 ($p<0.01$). Simultaneously, there was an elevation in the expression of the tumor protein 53 (TP53) compared to untreated control cells (Figure 3 and 4). These findings strongly indicate that AEV01 inhibits the proliferation of glioma and liver cancer cells, potentially through the modulation of inflammation and tumor suppression.

AEV01's Impact on CD36 Expression Across Glioma, Liver Cancer, and Senescence Cells

Building upon our preceding observations of AEV01's impact on inflammatory and tumor suppressor markers, our investigation extended to delve into the potential anti-tumor effects of AEV01, with a specific focus on examining the expression of CD36 in U-87MG

glioblastoma (GB) and HepG2 liver cancer cells. Employing Immunofluorescence (IF) analysis at 20X magnification, CD36 expression was visualized in green, while nuclei were counterstained using 4',6-diamidino-2-phenylindole (DAPI) (Figure 5). Notably, a significant downregulation of CD36 expression was observed in both U-87MG and HepG2 cells following treatment with AEV01, hinting at a potential mechanistic link to the observed anti-tumor effects (Figure 5: I and II).

To gain deeper insights into the role of CD36 in liver cancer cells, IF analysis was employed to scrutinize the metabolic alterations induced by palmitic acid (PA), a critical factor in hepatocellular carcinoma (HCC) pathogenesis. Both high and low doses of PA were found to promote CD36 expression (Figure 6B and C). Intriguingly, the administration of AEV01 (IC50) in combination with a high dose of PA resulted in a significant downregulation of CD36 compared to the untreated control cells (Figure 6E).

Furthermore, our study delved into exploring the senescence property induced by CD36 in human liver senescence cells (WRL-68). Utilizing IF analysis at 20X magnification, a positive control was considered (Figure 7-I and II), with DAPI counterstaining serving as a negative control. In coherence with our earlier findings, AEV01 was found to elevate CD36 expression (53.5%) compared to the untreated control (40%) senescence cells (Figure 7-III). While establishing a direct correlation between CD36 expression and senescence cell growth proved challenging due to limited studies, we interpreted the results in terms of proliferation percentage relative to CD36 expression levels (Figure 7-II and III). These intricate findings illuminate a complex interplay between CD36 expression and the effects of AEV01 on both liver cancer cells and senescence cells, prompting the need for further in-depth investigation.

Histopathological effects of AEV01 against glioma-induced xenograft model

Extending the thread of our preliminary *in vitro* findings, we sought to substantiate the anti-tumor potential of AEV01 using a glioma-induced animal model. Remarkably, the brain tissues from the tumor-control group exhibited the formation of mitotic cells with intra-hemorrhage lesions and dense nuclei, indicative of aggressive tumor characteristics. In contrast, healthy control tissues displayed a normal nuclear-cytoplasmic appearance with minimal signs of hemorrhage and the least mitotic cells (Figure 8-I and II).

Interestingly, upon histopathological staining analysis, AEV01-treated glioma-induced xenograft tissues demonstrated a morphological appearance similar to that of healthy control

tissues. This contrasted with the tumor-control group, showcasing a lower mitotic index and an absence of hemorrhage signs (Figure 8-III). Notably, the vehicle control did not exert any significant effect on tumor growth. These findings strongly suggest that AEV01 has the potential to restore the morphological appearances of tumor xenografts with minimal side effects.

In alignment with these *in vivo* observations, we further explored the immunohistochemical expression of CD36—a fatty acid translocase protein with implications in lipid metabolism and cellular reprogramming in cancer cells, including glioma. The IHC analysis of CD36 was conducted across each experimental group. In healthy control brain tissues, CD36 expression was minimal, while the tumor-control group exhibited elevated CD36 expression, evident by cytoplasmic positivity (Figure 9-I-b). Interestingly, AEV01-treated glioma tissues downregulated the expression of CD36 compared to both tumor-control and vehicle-control experimental groups (Figure 9-I b and c).

The cytoplasmic positivity of CD36 observed in AEV01-treated glioma tissues mirrored that of healthy control-treated groups (Table 1). Overall, AEV01 demonstrated a reduction in tumor growth formation, possibly mediated through the downregulated expression of CD36, in comparison to the tumor-control group ($p<0.01$), as supported by the IHC analysis. These results reinforce the potential therapeutic efficacy of AEV01 in glioma treatment, validated through both in vitro and in vivo studies.

Table 1: Immunohistochemical (IHC) scores of CD36 against each of the experimental groups

Treatment groups	Intensity	% Positivity	IHC scores (intensity × % positivity)
Healthy control	0	1	0
Tumor-control	2	2	4
AEV01-treated	1	2	2
Vehicle control	2	2	4

AEV01's Inhibitory Effects on Glioma Progression Through Modulation of Inflammatory Markers and TP53 Expression

In alignment with the compelling *in vivo* pathogenesis study outcomes, where AEV01 showcased a reduction in tumor growth formation and CD36 expression, we extended our investigation to the protein expression level using ELISA. The examination revealed that AEV01-treated glioma tissues demonstrated a downregulation in the expression of inflammatory markers, including IL-6, IL-18, IL-1β, TNF-α, CRP, and CASP-1 ($p<0.01$), alongside an elevated expression of the tumor protein 53 (TP53), in comparison to untreated control cells (Figure 10).

These results indicate that AEV01 hinders the propagation of tumor growth through the downregulation of inflammatory markers associated with inflammasome formation. Simultaneously, there is a concurrent upregulation of tumor protein 53 (TP53), a crucial tumor suppressor marker. The consistency across multiple levels of analysis, from histopathology to IHC and now to ELISA, further strengthens the evidence supporting AEV01's inhibitory effects on glioma progression.

Histopathological effects of AEV01 against HCC induced animal model

The present study aimed to explore the anti-hepatocellular potential of AEV01 in Hep3B-induced hepatocellular carcinoma model. As per our preliminary *in vitro* findings, AEV01 significantly altered the structural appearance of liver tissues as compared to tumor control. Upon exposure to AEV01, the tissue architecture was restored to that of normal healthy control as shown in Figure 11. As per the histopathological findings, liver tissue expressed formation of hemorrhagic lesions and poorly differentiated hepatocyte appearance, whereas, AEV01 treated tissues reverted towards a normal hepatocyte appearance (Figure 11A-III, B), while vehicle control didn’t exert any alterations in the tumor architecture and hence its efficacy is undermined to that of treated tissue (Figure 11A-IV, B).

Validation of *in vitro* findings through ELISA analysis in HCC-induced animal models

Following, exposure of HCC-induced tumor animals to AEV01 treatment, proteins isolated from tissue samples was eventually subjected to ELISA in order to validate the *in vitro* findings. It was observed that expression of inflammatory markers- IL6. IL-18, IL-1β, TNF-α, CRP and Casp-1 was reduced in AEV01-treated rats, whereas tumor protein 53 (TP53), expression was elevated when compared to tumor and vehicle-control, treated rats significantly (Figure 12).

Histopathological Analysis Shows AEV01's Safety and Anti-Tumor Effects in glioma and liver cancers

The preliminary study findings focused on assessment of anti-tumor potential of AEV01 against glioma and HCC cancer cells, wherein, apoptosis was triggered in these cancer cells mediated via downregulated expression of CD36, a key component contributing towards tumorigenesis process. On grounds of these, *in vivo* experiments were conducted, whereby, we observed that AEV01 impacted the growth of tumor mediated via downregulation of inflammatory markers against glioma and HCC-induced xenograft models. We observed that AEV01 significantly impacted tumor growth against both of these models. However, anti-tumor drugs/treatment are assumed to exert adverse side effects, thereby, histopathological analysis was performed to assess if any toxicity was induced against the vital organs. Interestingly, we observed that heart and lungs depicted normal cardiac muscle fibres and alveolar structures without any edema lesions (Figure 13 and 14-I). Likewise, liver tissues (glioma model) portrayed clear hepatocytes structures without any signs of fatty deposits or necrosis. Histopathological sections of kidney depicted clear and distinct visible nucleolus, without any necrotic infiltrations against all of the experimental groups (Figure 13 and 14-II). Similarly, photomicrographs of spleen and pancreas didn't exhibit any abrupt alterations in their morphological appearance. Above all, our study indicates that AEV01 is tolerable at its respective doses, while inducing pathological effect against the tumor xenograft model (Figure 13 and 14).

Discussion

Cancer is one of the leading causes of death across worldwide. Amongst all of the cancer reported, glioma or glioblastoma multiforme (GBM, grade IV form of glioma), is rarest, yet one of the dreadful forms of brain tumor. On the other hand, liver cancer or adenocarcinoma in liver is the fifth leading cause of death in India and across worldwide (1). The rising concern of mortality cases due to cancer has necessitated the dire need to implement alternative therapeutic strategies.

Synthetic compounds namely, cis-platin or taxol, doxorubicin or other drug conjugates such as sorafenib, imatinib have been the gold-standard regimens to treat most of the cancers including glioma and liver (2). Unfortunately, most of these therapeutic agents inflicted with adverse side-effects. Contemporarily, natural products have emerged as crucial and key therapeutic agents. As an instance, curcumin, which is originated from Indian spice,

demonstrated potent anti-tumor activities in several cancers including breast, colon, lungs, liver and glioma (3). Likewise, extracts derived from medicinal plants such as tulsi, exhibited potent anti-tumor effects in most of the cancers (4). However, there are lacunae of studies reporting on the possible transition of these therapeutic ailments from bench to bedside.

Picrorhiza Kurroa (*P.kurroa*) is a medicinal herb, which exhibited several bioactivities such as anti-pyretic, anti-parasitic, hepatoprotective, anti-inflammatory, anti-carcinogenic. However, there are paucity of studies reported on the pharmacological activities of derivatives obtained from *P.kurroa* (5). *P.kurroa* constitutes several active components, namely, a steroidal glycoside, Cucurbitacins B, D, and R, isolated from its roots, which attributes to its potent anti-tumor and cytotoxic effects (5).

In the present study, AEV01, a speciality extract from *P.kurroa*, has demonstrated potent cytotoxicity in U-87MG GB and HepG2/Hep3B liver cancer cells, but to the least in human embryonic kidney cells, i.e HEK293T, which corroborates with one of the similar study, wherein, picroliv (a purified iridoid glycoside fraction from roots of *Picrorhiza kurrooa*) exhibited anti-cancer properties against Hep3B and Glioma cells (6). Further, the examination of apoptosis induction by AEV01 at morphological levels on U-87MG and HepG2 cells was conducted using AO/EtBr dual stain. AO, being permeable to live cells, appears green, while cells in the early stage of apoptosis exhibit yellow-green fluorescence. On the other hand, EtBr stains dead cells, particularly those in the late stage of apoptosis, producing an orange-red fluorescence. In this study, the treatment with AEV01 on both U-87MG and HepG2 cells significantly induced apoptosis, with percentages measured at 24.5% and 59.59%, respectively. Remarkably, the vehicle control (VC, Figure 2: I and IIC) demonstrated that over 90% of cells in both U-87MG and HepG2 cells remained viable. This observation indicates that the vehicle control did not elicit apoptosis in these cells. The lack of apoptosis induction in the vehicle control provides a crucial baseline for comparison with the AEV01-treated groups. This result suggests that any observed apoptotic effects in the AEV01-treated cells are specific to the treatment and not merely a consequence of the experimental conditions or vehicle used.

The absence of significant apoptosis in the vehicle control groups underscores the specificity of AEV01 in triggering apoptotic pathways in U-87MG and HepG2 cells. These findings enhance the credibility of the observed apoptotic effects in the treated groups, reinforcing the

notion that AEV01 possesses anti-tumor properties by inducing programmed cell death in these cancer cells.

In line with the previously observed significant induction of apoptosis in the dual-staining results, the current study was further focused on the modulation of inflammatory and tumor suppressor markers. Previous studies reported that extracts or secondary metabolites derived from *P.kurroa* exerted potent anti-inflammatory effects, via downregulation of TNF-α, IL-6/18 or IL-1β (8). The results demonstrated a compelling downregulation in the expression of various inflammatory markers, including IL-6, IL-18, IL-1β, TNF-α, CRP, and CASP-1, in AEV01-treated glioma and liver cancer cells (Figure 3 & 4). This significant reduction in inflammatory markers is consistent with the cytotoxic effects observed in the initial evaluation of AEV01. The cytotoxicity results highlighted the potent impact of AEV01 on U-87MG glioma and Hep3B liver cancer cells, affirming its potential as an effective anti-cancer agent. Moreover, the observed downregulation of inflammatory markers aligns with the apoptotic effects induced by AEV01, as evidenced by the increased formation of apoptotic cells in both cancer cell lines.

Apoptosis, a fundamental process that regulates cell death in a controlled manner, is often dysregulated in cancer cells, contributing to tumorigenesis. The ability of AEV01 to induce apoptosis suggests a targeted and controlled approach toward inhibiting the proliferation of glioma and liver cancer cells. Simultaneously, the elevation in the expression of the tumor protein 53 (TP53) in AEV01-treated cells further strengthens the anti-cancer effects of AEV01. TP53, a crucial regulator of cell cycle progression and a well-known tumor suppressor, plays a pivotal role in preventing the uncontrolled growth of cancer cells. The upregulation of TP53 suggests that AEV01 not only induces apoptosis but also exerts its effects through the activation of key tumor suppressor pathways.

CD36, recognized as a pivotal marker for cancer stem cells, exhibits heightened expression across various cancers, including glioblastoma and liver cancer, portraying its role as pro-tumorigenic in cancer stem cells (CSCs) (10). Notably, its expression strongly correlates with the tumor progression of hepatocellular carcinoma (HCC), where its overexpression contributes to increased growth, proliferation, migration, and invasion (11). CD36 also plays a role in altering the metabolic state by inducing oncogenic glycolysis over oxidative phosphorylation (11). Additionally, CD36 is associated with a tumor-promoting phenotype characterized by immunosuppressive and pro-inflammatory activities. Studies have reported

that elevated CD36 expression is linked to increased levels of tumor-infiltrating macrophages, thereby suppressing anti-inflammatory activities in HCC (12), suggesting CD36 as a potential anti-tumor therapeutic target.

In the present study, immunofluorescence (IF) was utilized to examine CD36 expression in U-87MG glioblastoma and HepG2 liver cancer cells (detected in green coloration, 20X magnification, Figure 5). Nuclei were counterstained with 4'6-diamidino-2-phenylindole (DAPI, 20X magnification, Figure 5). One plausible mechanism for the anti-tumor effects of AEV01 could be attributed to the downregulated expression of CD36 (Figure 5 I and II).

Further exploration of CD36 expression in liver cancer cells involved IF to investigate the metabolic alterations induced upon administration of PA, a critical factor in the pathogenesis of HCC, regulating immune responses, glucose, and lipid metabolism. The study observed a significant downregulation of CD36 expression upon administration of AEV01 (IC50) in combination with a high dose of PA, compared to the control (Figure 6E). This downregulation of CD36 with AEV01 might be linked to the lipotoxicity induced by PA, leading to pyroptosis, as evidenced by the upregulated expression of caspase-1 and IL-1β in HCC (13). While apoptosis was evident, upon administration of AEV01 in combination with PA requires validation at the transcriptional and translational levels.

Senescence, a unique pattern of cell death, plays a paradoxical role in tumorigenesis. Various markers, including lipids, fatty acids, or protein biomolecules, regulate senescence, modulating processes such as tumor suppression, metastasis, and aging (14). In this study, IF was employed to examine CD36 expression in human liver senescence cells-WRL-68 (detected in green coloration, 20X magnification, considered as a positive control, figure 7-I and II), with nuclei counterstained with DAPI (20X magnification, considered as a negative control, Figure 7-I and II). Continuing from previous study findings, AEV01 was observed to elevate CD36 expression (53.5%) compared to the control (40%), potentially regulating the proliferation capacity of senescence cells (Figure 7-III). While a direct correlation between the growth of these senescence cells could not be drawn, further interpretation in terms of proliferation (%) was executed with respect to the expression levels of CD36 (Figure 7-II and III). The upregulated expression of CD36 in senescence cells under therapeutic exposure remains debatable, as senescence can either downregulate tumor suppressor genes or provoke the synthesis of proto-oncogenes (15). Thus, the downregulation of CD36 observed in

glioblastoma and liver cancer cells, particularly in the context of metabolic alterations induced by AEV01 and PA combination, presents a promising avenue for anti-tumor therapeutic interventions.

Building upon the initial *in vitro* results, which delved into the potential anti-tumor effects of AEV01 on cancer cells by suppressing inflammatory markers and increasing the formation of apoptotic cells, our next step involved validating these experimental findings. To do so, we examined the anti-tumor efficacy of AEV01 in orthotopic xenograft-induced glioma model. Previously reported studies stated that, upon inducing 20-methylcholanthrene (20 MC) in mice model, sarcoma developed, but administration of *Picrorrhiza kurroa* extracts suppressed formation of transplanted tumors with an enhancement of life-span in mice model (16). Also, ethanolic/methanolic extracts of *Picrorrhiza kurroa* have demonstrated effective anti-tumor activities in several tumor-induced animal models. Apart from tumoricidal activities, it mediates immunological responses against diverse set of diseases. In accordance with our previous *in vitro* findings, it was observed in a study, wherein, a bioploymeric function of *P. kurroa* served as potent immune-modulator, enhanced expression of humoral and cell-mediated immune responses in animal model (5). Lou et al reported that extracts of *P. kurroa* inhibited proliferation, migration and invasion of human breast cancer cells. Additionally, it exerted anti-angiogeneic and anti-metastatic activities in lung cancer xenograft model via retraced tube formation mediated by human endothelial cells (HUVECs) and cell-adhesion metastasis (CAM) (17). In line with the aforementioned study results, we observed that tumor control groups displayed the development of mitotic cells with intra-haemorrhage lesions and dense nuclei. In contrast, healthy control tissues exhibited a normal nuclear-cytoplasmic appearance, devoid of any signs of haemorrhage, and had the lowest occurrence of mitotic cells (Figure 8-I and II). Notably, the histopathological staining analysis of glioma-induced xenograft tissues treated with AEV01 revealed a morphological appearance similar to that of the healthy control, as opposed to the tumor control. Additionally, the AEV01-treated group exhibited a lower mitotic index and showed no signs of haemorrhage (Figure 8-III). In contrast, the vehicle control did not exert any effect on tumor growth. These findings suggest that AEV01 has the potential to restore the morphological features of tumor xenografts with minimal side effects.

Moreover, we delved into the immunohistochemical expression of CD36, a fatty acid translocase protein pivotal in lipid metabolism, thereby influencing cellular reprogramming

in cancer cells, including glioma. CD36 expression correlates with tumorigenic processes and governs the metabolic profile of these cancer cells (4).

To investigate this aspect, immunohistochemistry (IHC) for CD36 was conducted across all experimental groups. Notably, minimal CD36 expression was observed in the healthy control, while the tumor control exhibited elevated CD36 expression, as indicated by cytoplasmic positivity (Figure 9-I-b). Intriguingly, our findings revealed that AEV01-treated glioma tissues demonstrated a downregulation in CD36 expression compared to both the tumor control and vehicle control experimental groups (Figure 9-b and c). The cytoplasmic positivity of CD36 in AEV01-treated glioma tissues resembled that of the healthy control-treated groups (Table 1). Overall, AEV01 significantly reduced tumor growth formation by downregulating CD36 expression compared to the tumor control ($p<0.01$), as evident from the IHC analysis.

Building upon the consistent outcomes observed in the previous in vivo study, where AEV01 exhibited a reduction in tumor growth formation and downregulated CD36 expression, the present investigation aimed to explore the effects of AEV01 at the protein expression level using ELISA. Our observation revealed the downregulation of inflammatory markers, including IL-6, IL-18, IL-1β, TNF-α, CRP, and CASP-1, following AEV01 treatment, suggesting a targeted inhibition of key pathways associated with tumorigenesis and inflammation (Figure 10). Notably, the elevated expression of tumor protein P53(TP53), a crucial tumor suppressor protein, further reinforces the anti-cancer effects of AEV01. The consistent reduction in tumor growth and inflammatory marker expression in glioma tissues, as demonstrated in both experimental settings, strengthens the credibility of our findings. The ability of AEV01 to induce apoptosis in glioma cells underscores its potential as a therapeutic agent. Apoptosis, a fundamental process that, when dysregulated, contributes to tumorigenesis. By promoting apoptosis, AEV01 exhibits a targeted and controlled approach towards inhibiting glioma cell proliferation. Thus, our study positions AEV01 as a promising and potent anti-tumor agent against glioma. The dual impact on inflammatory markers and apoptotic pathways suggesting a multifaceted mechanism of action.

The study also demonstrated AEV01's potential as an anti-hepatocellular carcinoma (HCC) agent in a Hep3B-induced model. *In vitro* results revealed AEV01's ability to restore liver tissue architecture to a normal state, reversing hemorrhagic lesions and poorly differentiated

hepatocyte appearance characteristic of HCC. Histopathological findings further support this, with AEV01-treated tissues displaying a shift towards normal hepatocyte appearance compared to the vehicle control group (Figure 11).

Moreover, translational insights from animal models confirm these observations. ELISA analysis of tissue samples reveals a reduction in inflammatory marker expression (IL6, IL-18, IL-1β, TNF-α, CRP, and Casp-1) and an elevation in tumor protein P53(TP53) expression following AEV01 treatment (Figure 12). These results suggest AEV01's potential to modulate inflammatory pathways and induce tumor-suppressive effects in vivo. Thus, these findings highlight AEV01 as a promising candidate for HCC therapy, warranting further investigation into its mechanisms of action and potential clinical applications.

Further, one of the critical considerations in evaluating the suitability of a potential anti-cancer drug is its safety profile. The histopathological analysis conducted in this study provides valuable insights into the potential toxicity of AEV01 on vital organs for both glioma-induced and HCC-induced rats. Remarkably, the examination of heart, lungs, liver, kidneys, spleen, and pancreas tissues revealed no significant abnormalities or adverse effects associated with AEV01 administration (Figure 13 & 14). This observation is particularly encouraging as it indicates the tolerability of AEV01 at the doses tested, suggesting a favorable safety profile for further clinical development.

The absence of histopathological alterations in the vital organs underscores the selectivity of AEV01 towards cancer cells, minimizing the risk of off-target effects commonly associated with traditional chemotherapeutic agents and radiation therapy. These findings support the continued investigation of AEV01 as a promising candidate for the treatment of glioma and HCC, highlighting its potential as a safer and more effective alternative to existing therapies.

Though *in vitro* and *in vivo* studies conducted by us, NASH-STAM animal studies conducted in Japan (unpublished data) and COVID-19 human studies conducted on AEV01 established a proof-of-concept safety and efficacy of AEV01 usage. However, further studies are warranted to elucidate the precise molecular mechanisms underlying the anti-tumor effects of AEV01 and to evaluate its long-term safety and efficacy in preclinical and clinical settings. Additionally, comprehensive pharmacokinetic and pharmacodynamic studies are essential to optimize dosing regimens and maximize therapeutic benefits while minimizing any possible ~~potential~~ adverse effects. Overall, the findings of this study contribute to the growing body of

evidence supporting the therapeutic potential of AEV01 in cancer treatment and warrant further exploration in future research endeavors.

Conclusion

In conclusion, this study underscores the critical need for alternative therapeutic strategies in combating the global menace of cancer, particularly in the context of glioma and hepatocellular carcinoma (HCC). The rising mortality rates associated with conventional synthetic compounds have prompted a shift towards exploring natural products as potential anti-cancer agents. AEV01, a specialty extract from *Picrorhiza Kurroa*, demonstrated potent cytotoxicity against U-87MG glioblastoma and HepG2 liver cancer cells, while sparing human embryonic kidney cells (HEK293T). The anti-tumor effects of AEV01 were attributed to its ability to downregulate CD36 expression, a crucial marker in glioblastoma and liver cancer, and induce apoptosis in cancer cells. The observed anti-inflammatory effects of AEV01, possibly mediated through the modulation of CD36 and tumor protein P53 (TP53) simultaneously, further contribute to its therapeutic potential. Immunofluorescence studies revealed a downregulation of CD36 expression in liver cancer cells treated with AEV01, particularly when exposed to palmitic acid (PA), indicating a potential mechanism for combating lipotoxicity-induced pyroptosis. Interestingly, in senescence cells, AEV01 exhibited an upregulation of CD36 expression, suggesting a nuanced role in regulating proliferation capacity. Further, the *in vivo* orthotopic xenograft-induced glioma model and HCC- induced model demonstrated that AEV01 not only inhibited tumor growth but also restored morphological features resembling healthy control tissues. Immunohistochemical analysis confirmed the downregulation of CD36 expression in glioma tissues treated with AEV01. Consistent with these findings, ELISA results demonstrated the downregulation of inflammatory markers and the upregulation of TP53 in glioma and liver tissues treated with AEV01. The multifaceted impact on inflammatory markers and apoptotic pathways highlights AEV01 as a promising anti-tumor agent against glioma. This comprehensive study, encompassing *in vitro* and *in vivo* experiments, provides valuable insights into the potential therapeutic efficacy of AEV01 derived from *Picrorhiza Kurroa*. The observed anti-tumor effects, coupled with its ability to modulate key molecular pathways, position AEV01 as a promising candidate for further exploration in clinical settings. Interestingly, AEV01 didn't exert any gross histopathological changes or alterations against the vital organs in either of tumor xenograft models. Hence, future research should focus on elucidating the pharmacokinetics profiling of AEV01, specific molecular mechanisms impacted by AEV01

and assessing its safety and efficacy in human trials, paving the way for a novel and effective therapeutic strategy against glioma and hepatocellular carcinoma.

References:

1. Mathur P, Sathishkumar K, Chaturvedi M, Das P, Sudarshan KL, Santhappan S, et al. Cancer Statistics, 2020: Report From National Cancer Registry Programme, India. JCO Glob Oncol. 2020 Jul;6:1063–75.
2. Gilad Y, Gellerman G, Lonard DM, O'Malley BW. Drug Combination in Cancer Treatment—From Cocktails to Conjugated Combinations. Cancers (Basel). 2021 Feb 7;13(4):669.
3. Sharifi-Rad J, Rayess YE, Rizk AA, Sadaka C, Zgheib R, Zam W, et al. Turmeric and Its Major Compound Curcumin on Health: Bioactive Effects and Safety Profiles for Food, Pharmaceutical, Biotechnological and Medicinal Applications. Front Pharmacol. 2020 Sep 15;11:01021.
4. Hasan MR, Alotaibi BS, Althafar ZM, Mujamammi AH, Jameela J. An Update on the Therapeutic Anticancer Potential of Ocimum sanctum L.: "Elixir of Life." Molecules. 2023 Jan 25;28(3):1193.
5. Almeleebia TM, Alsayari A, Wahab S. Pharmacological and Clinical Efficacy of Picrorhiza kurroa and Its Secondary Metabolites: A Comprehensive Review. Molecules. 2022 Jan;27(23):8316.
6. Gaddipati JP, Madhavan S, Sidhu GS, Singh AK, Seth P, Maheshwaril RK. Picroliv - a natural product protects cells and regulates the gene expression during hypoxia/reoxygenation. Mol Cell Biochem. 1999 Apr 1;194(1):271–81.
7. Rathee D, Thanki M, Bhuva S, Anandjiwala S, Agrawal R. Iridoid glycosides-Kutkin, Picroside I, and Kutkoside from Picrorrhiza kurroa Benth inhibits the invasion and migration of MCF-7 breast cancer cells through the down regulation of matrix metalloproteinases: 1st Cancer Update. Arabian Journal of Chemistry. 2013 Jan 1;6(1):49–58.
8. Kumar R, Gupta YK, Singh S, Raj A. Anti-inflammatory Effect of Picrorhiza kurroa in Experimental Models of Inflammation. Planta Med. 2016 Nov;82(16):1403–9.
9. Rajkumar V, Guha G, Ashok Kumar R. Antioxidant and anti-neoplastic activities of Picrorhiza kurroa extracts. Food and Chemical Toxicology. 2011 Feb 1;49(2):363–9.

10. Hale JS, Otvos B, Sinyuk M, Alvarado AG, Hitomi M, Stoltz K, et al. Cancer Stem Cell-Specific Scavenger Receptor CD36 Drives Glioblastoma Progression. Stem Cells. 2014 Jul 1;32(7):1746–58.

11. Luo X, Zheng E, Wei L, Zeng H, Qin H, Zhang X, et al. The fatty acid receptor CD36 promotes HCC progression through activating Src/PI3K/AKT axis-dependent aerobic glycolysis. Cell Death Dis. 2021 Mar 26;12(4):328.

12. Yang P, Qin H, Li Y, Xiao A, Zheng E, Zeng H, et al. CD36-mediated metabolic crosstalk between tumor cells and macrophages affects liver metastasis. Nat Commun. 2022 Oct 2;13(1):5782.

13. Zeng X, Zhu M, Liu X, Chen X, Yuan Y, Li L, et al. Oleic acid ameliorates palmitic acid induced hepatocellular lipotoxicity by inhibition of ER stress and pyroptosis. Nutrition & Metabolism. 2020 Jan 30;17(1):11.

14. Hamsanathan S, Gurkar AU. Lipids as Regulators of Cellular Senescence. Frontiers in Physiology [Internet]. 2022 [cited 2024 Jan 10];13. Available from: https://www.frontiersin.org/articles/10.3389/fphys.2022.796850

15. Cai X, Guillot A, Liu H. Cellular Senescence in Hepatocellular Carcinoma: The Passenger or the Driver? Cells. 2022 Dec 29;12(1):132.

16. Joy KL, Rajeshkumar NV, Kuttan G, Kuttan R. Effect of Picrorrhiza kurroa extract on transplanted tumours and chemical carcinogenesis in mice. Journal of Ethnopharmacology. 2000 Jul 1;71(1):261–6.

17. Lou C, Zhu Z, Xu X, Zhu R, Sheng Y, Zhao H. Picroside II, an iridoid glycoside from Picrorhiza kurroa, suppresses tumor migration, invasion, and angiogenesis in vitro and in vivo. Biomedicine & Pharmacotherapy. 2019 Dec 1;120:109494.

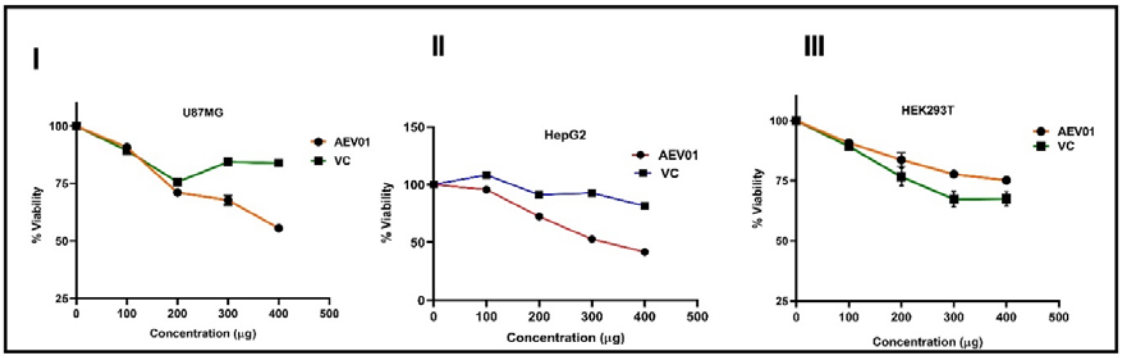

Figure 1: Cell viability assay by MTT on U-87MG GB, HepG2 liver cancer and HEK293T cells

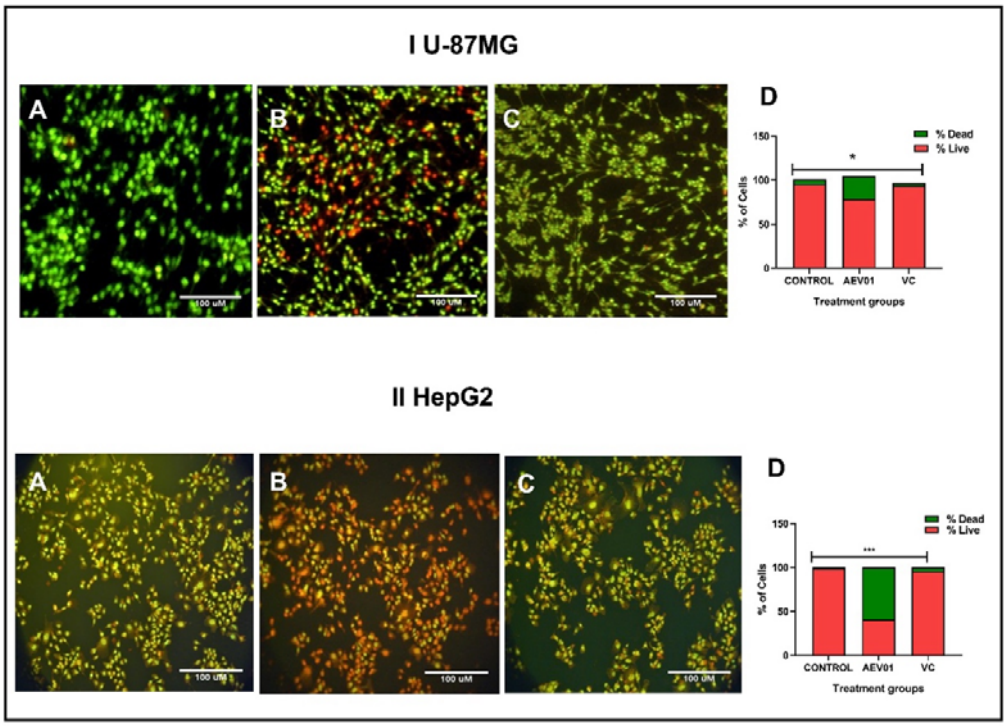

Figure 2: Apoptotic cell death was observed by AO/EtBr staining under different experimental treatment groups on I-U-87MG glioma and II-HepG2 liver cancer cells (A) Control, (B) AEV01-treated (C) Vehicle-control, (D) Percentage of apoptotic cells were measured by scoring viable and dead cells. * and *** indicates $p<0.05$ & $p<0.001$ in comparison to untreated control, respectively.

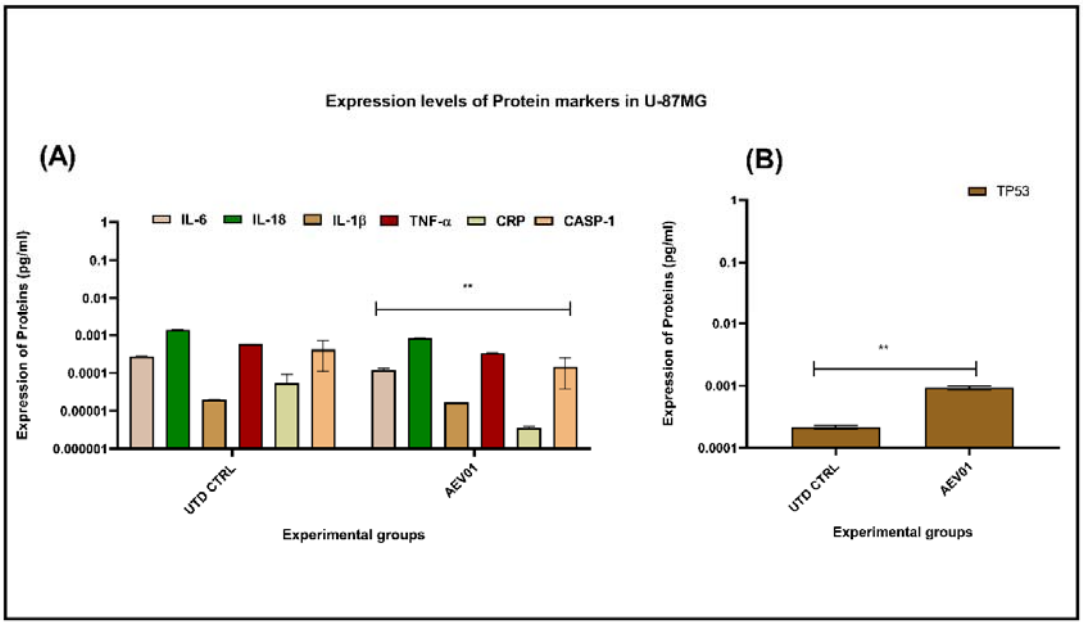

Figure 3: Anti-glioma effects of AEV01 (Logarithmic scale base 10) of inflammatory markers (A) IL-6, IL-18, IL-1β, TNF-α, CRP, CASP-1 and (B) tumor protein P53 (TP53) in U-87MG cells, ** indicates p<0.001 in comparison to untreated-control (UTD CTRL)

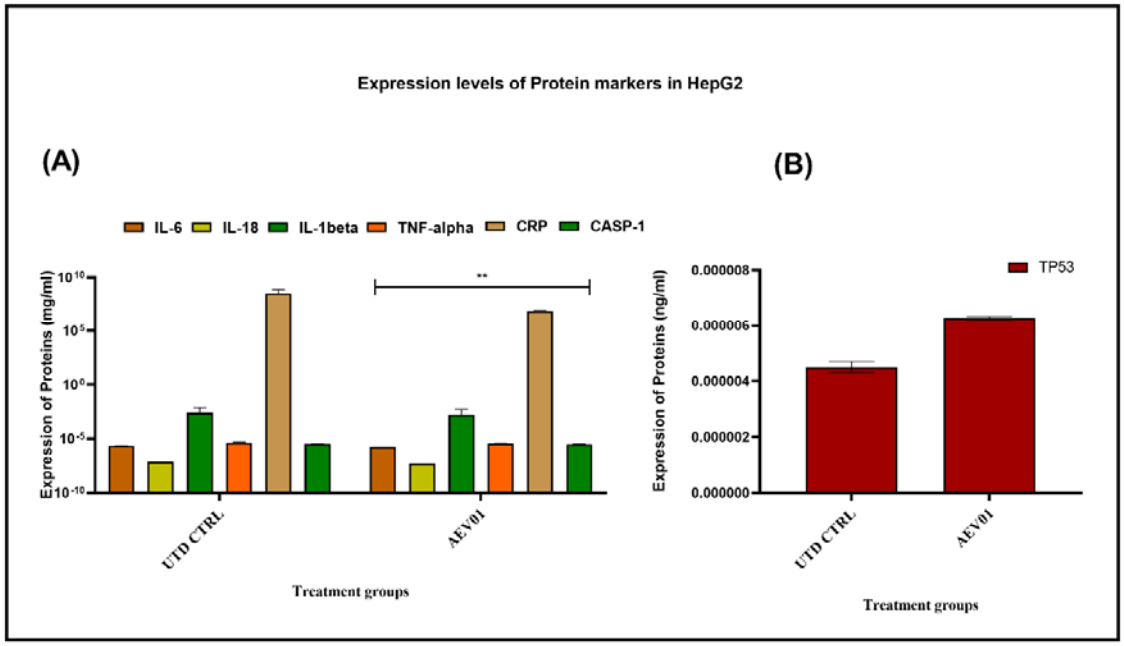

Figure 4: Anti-tumor effects of AEV01 (Logarithmic scale base 10) of inflammatory markers (A) IL-6, IL-18, IL-1β, TNF-α, CRP, CASP-1 and (B) tumor protein P53 (TP53) in HepG2 liver cancer cells (Linear scale), ** indicates p<0.001 in comparison to untreated, control (UTD CTRL)

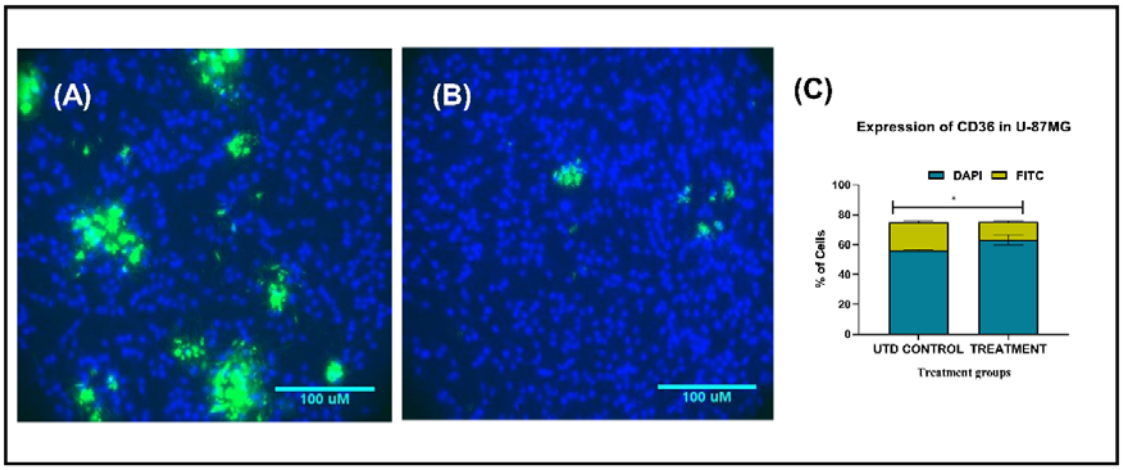

Figure 5: Immunofluorescence (IF) depicted that CD36 (green) was expressed in I-U-87MG glioma and II-HepG2 liver cancer cells, whereas, nuclei was counter-stained with DAPI (blue), (A) Untreated, control, (B)AEV01-Treated, * and *** indicates p<0.05.

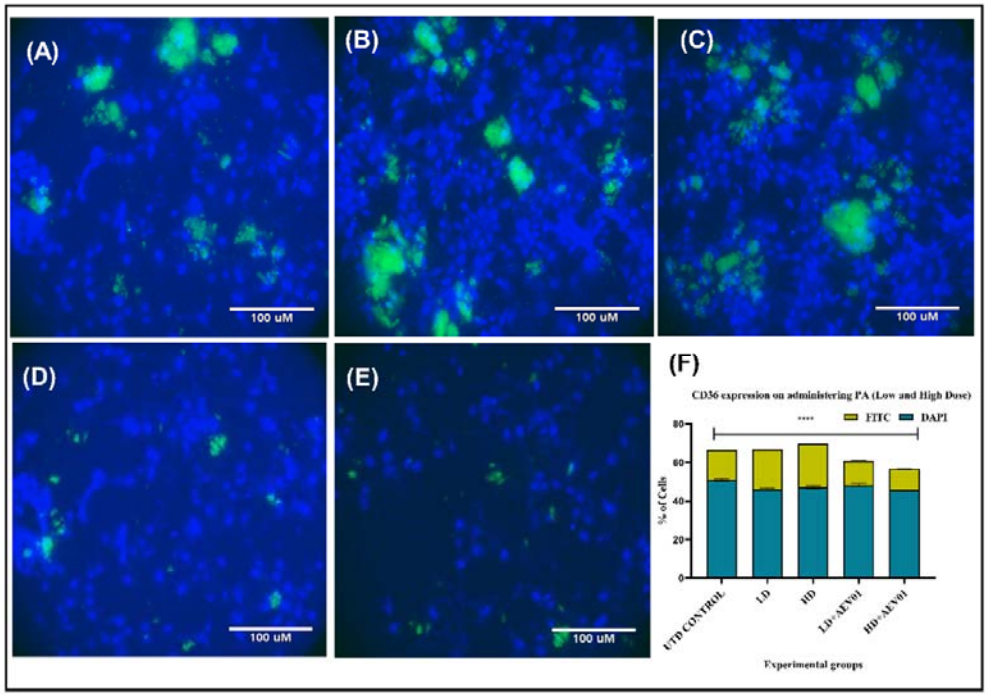

Figure 6: Immunofluorescence (IF) based evaluation of CD36 expression under low and high doses of PA, as individually and in combination with AEV01n in HepG2 liver cancer cells, whereas, nuclei was counter-stained with DAPI (blue), (A) untreated control, (B)- PA Low dose (LD) treated, (C)- PA High dose (HD) treated, (D)- PA LD +AEV01 (IC50), (E)-PA HD +AEV01 (IC50) **** indicates p<0.0001.

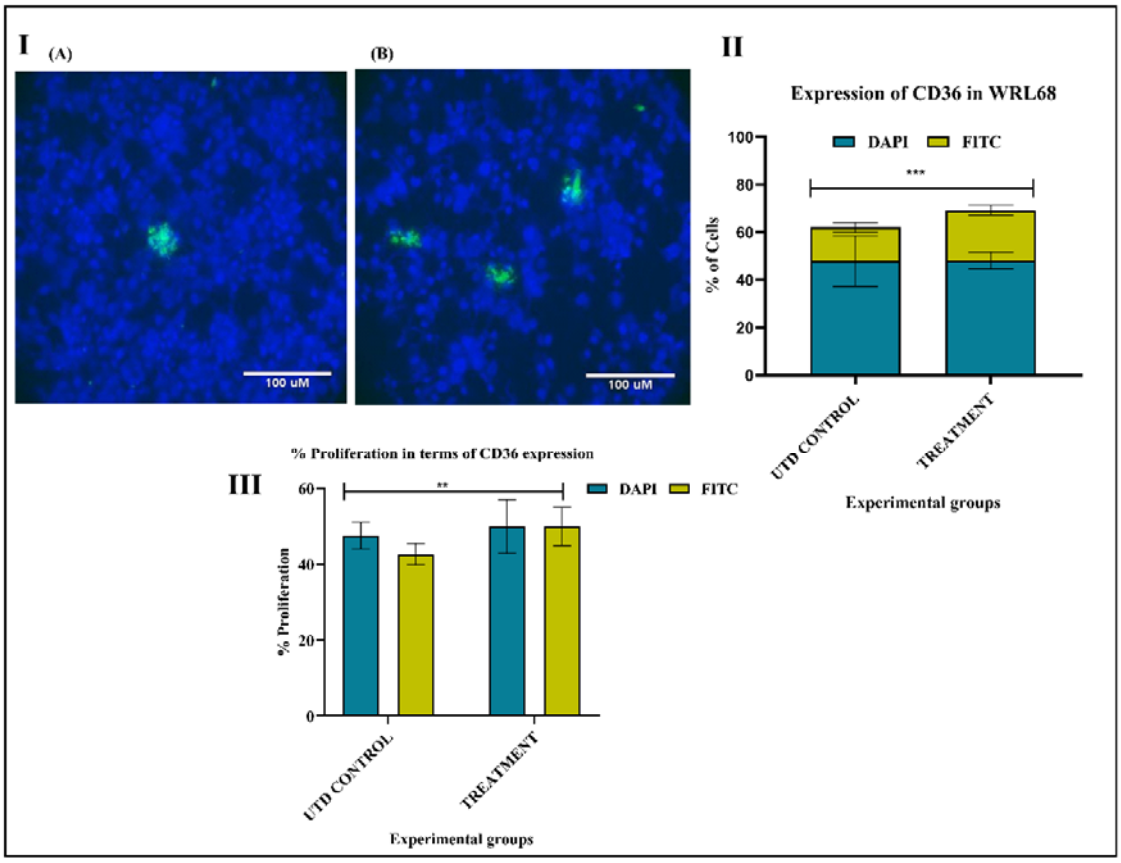

Figure 7: I-Immunofluorescence (IF) depicted that CD36 (green) was expressed in human liver senescence cells (WRL-68), whereas, nuclei was counter-stained with DAPI (blue), (A) Untreated control (UTD CTRL) (B)-Treated, II- Clustered analysis of DAPI and FITC against untreated control and AEV01 treatment, III- % Proliferation interpreted in terms of CD36 expression, ** and *** indicates $p<0.05$.

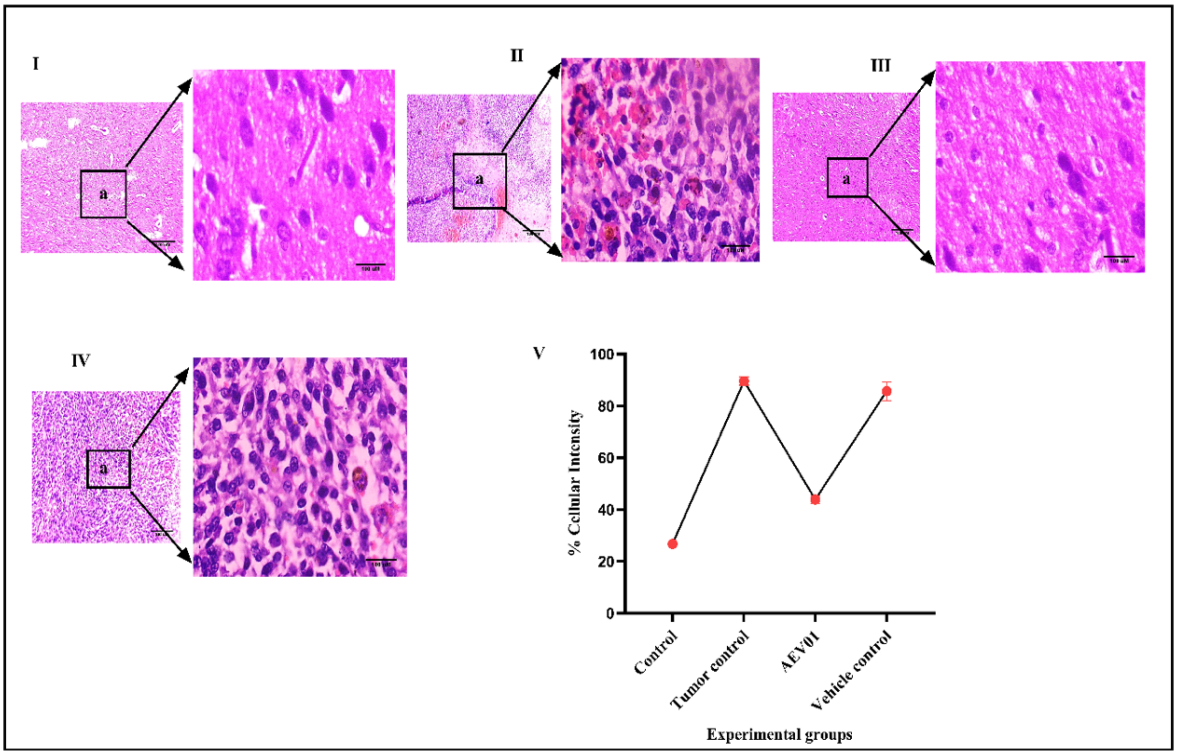

Figure 8: Histopathological analysis of different experimental groups: **I**-healthy control, **II**- Glioma induced tumor control, **III**-AEV01-treated in glioma induced model, **IV**- vehicle control in glioma induced model, **V**- Quantitative analysis of H and E-stained tissues against each of the experimental groups by ImageJ.

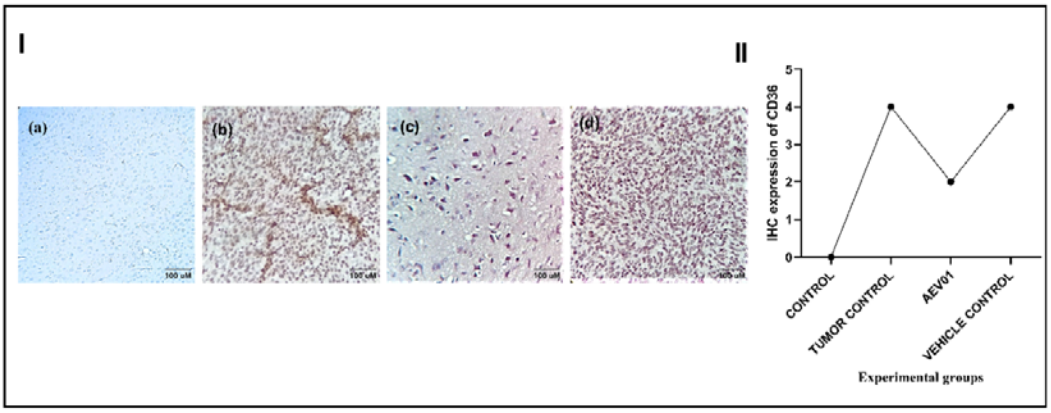

Figure 9: I-Immunohistochemistry (IHC) of CD36 against different experimental groups: **(a)** healthy control, **(b)** tumor control, **(c)** AEV01-treated in glioma induced model, **(d)** vehicle control in glioma induced model, **II**-Quantitative analysis of IHC scores based on patterns of expression of CD36 against each of the experimental groups by Image J.

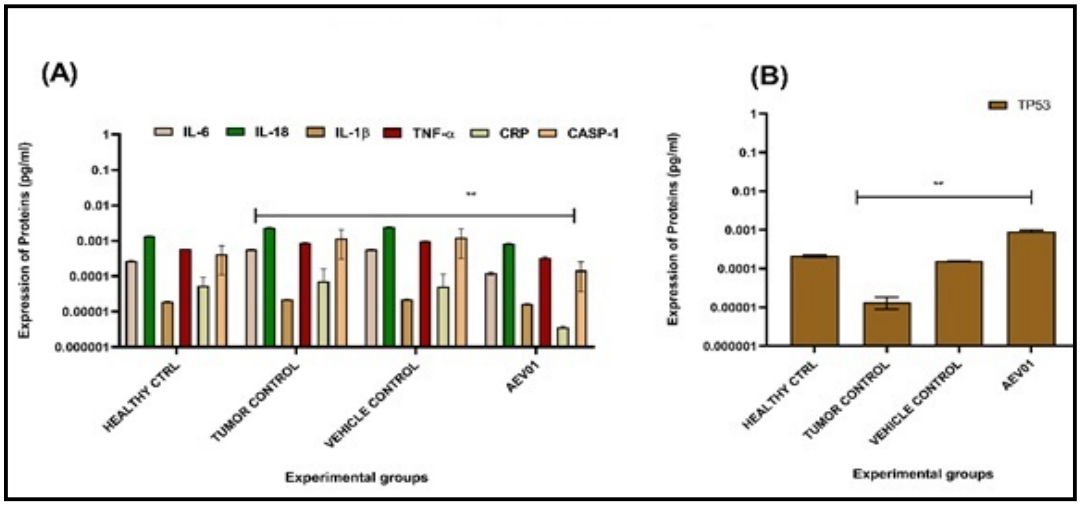

Figure 10: Anti-glioma effects of AEV01 (Logarithmic scale base 10) of inflammatory markers (A) IL-6, IL-18, IL-1β, TNF-α, CRP, CASP-1 and (B) tumor suppressor protein P53 (TP53) in U-87MG implanted glioma model, ** indicates p<0.001 in comparison to control

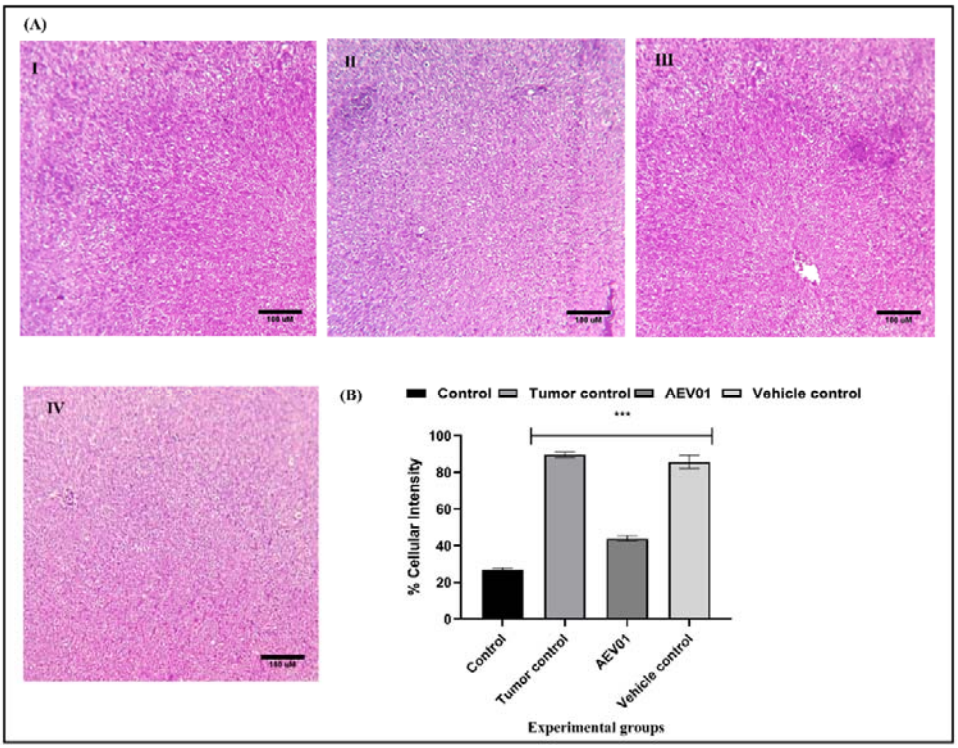

Figure 11:

(A)-Histopathological analysis of AEV01 against Hep 3B- induced hepatocellular carcinoma model (HCC)- I- Healthy control, II-tumor control, III- AEV01 treated, IV- Vehicle control; **(B)-**Quantification was performed using ImageJ, ***p<0.001 was considered as statistically significant.

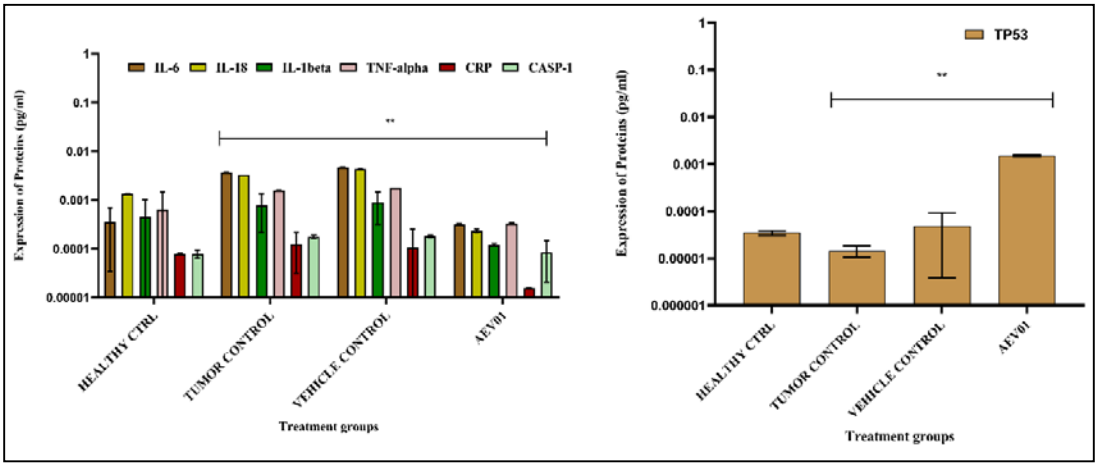

Figure 12: Anti-tumor effects of AEV01 in HCC- induced liver tissue samples by ELISA. Down & up regulation of inflammatory and tumor protein markers, respectively in AEV01 tissue samples with respect to control significantly (** indicates $p<0.01$, with respect to control).

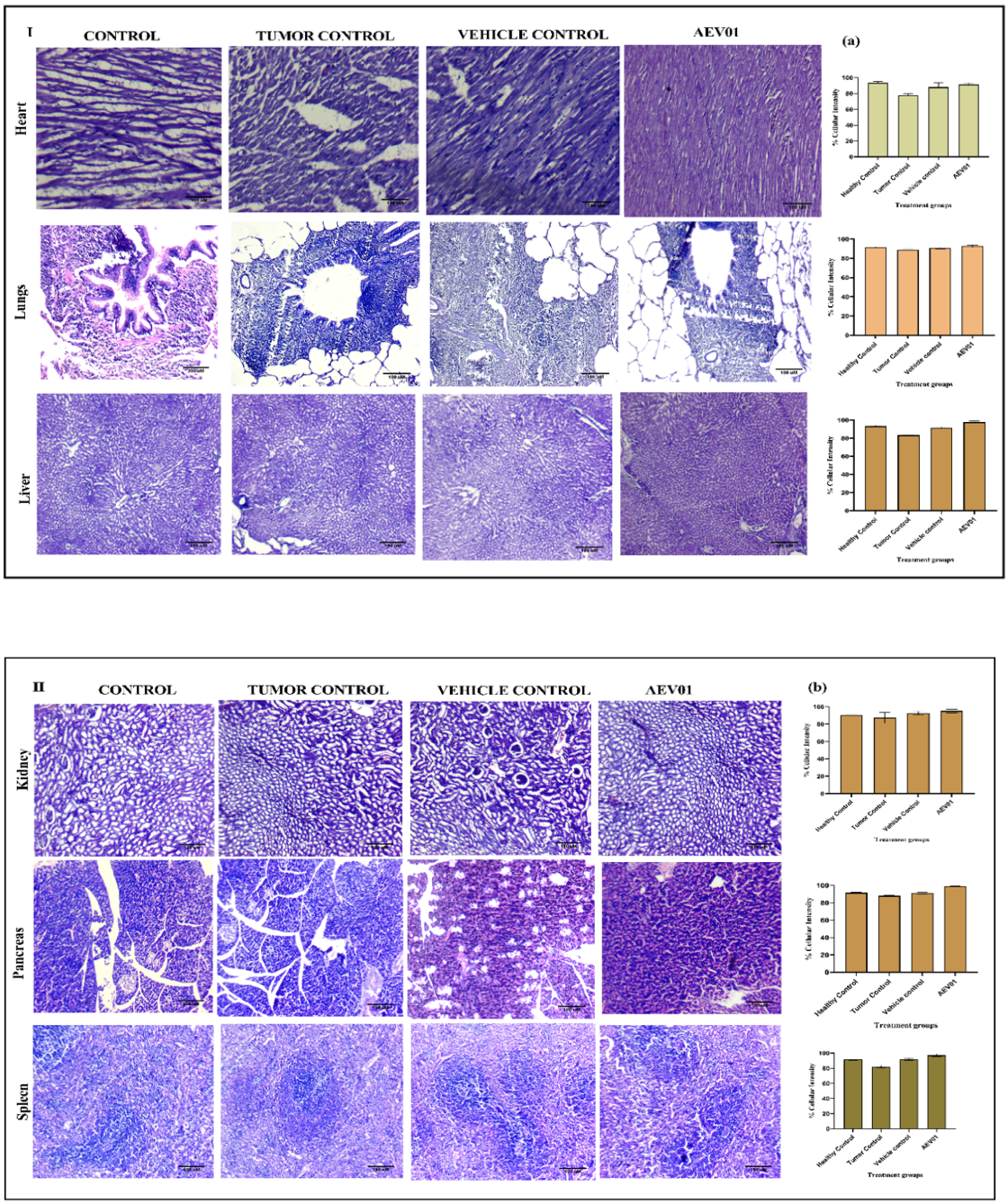

Figure 13: I and II- Histopathological examination on the vital organs of glioma-induced, AEV01-treated rats such as heart, lungs, liver, pancreas, spleen and kidney were quantified at 40x magnifications by inverted microscope (b) quantitative data based on the cellularity index was obtained employing ImageJ. Data are represented in terms of mean ± SD, n=3.

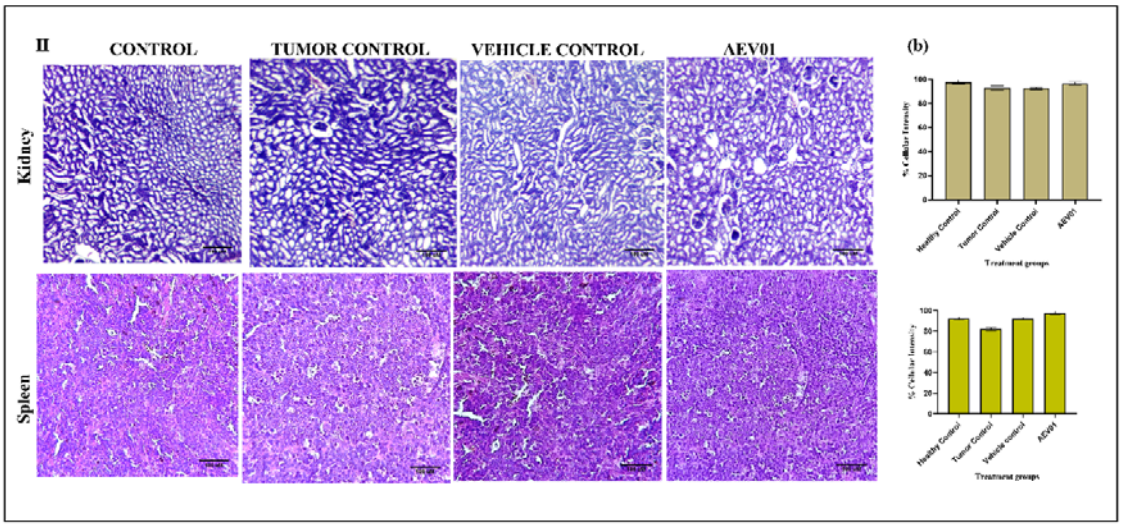

Figure 14: I and II- Histopathological examination on the vital organs of HCC (Hep3B)-induced, AEV01-treated rats such as heart, lungs, pancreas, kidney and spleen were quantified at 40x magnifications by inverted microscope (b) quantitative data based on the cellularity index was obtained employing ImageJ. Data are represented in terms of mean ± SD, n=3.